Single Photon-Induced Symmetry Breaking of H2 Dissociation

F. Martín, *et al.*

Science **315**, 629 (2007);
DOI: 10.1126/science.1136598

Science (print ISSN 0036-8075; online ISSN 1095-9203) is published weekly, except the last week in December, by the American Association for the Advancement of Science, 1200 New York Avenue NW, Washington, DC 20005.

not conformational motions after photoexcitation (*6*, *39*), determines the outcome of a reaction. Flexibility does not help an excitation at a bipyrimidine doublet attain a better conformation within its lifetime, but a more flexible backbone can increase the fraction of reactive conformations that are present at the time of light absorption. With knowledge about the conformational criteria that make reaction inevitable, molecular-dynamics simulation can be used to identify damage hot spots.

References and Notes

1. J. Cadet, P. Vigny, in *Bioorganic Photochemistry*, H. Morrison, Ed. (Wiley, New York, 1990), pp. 1–272.
2. J. S. Taylor, *Acc. Chem. Res.* **27**, 76 (1994).
3. A. A. Vink, L. Roza, *J. Photochem. Photobiol. B Biol.* **65**, 101 (2001).
4. V. O. Melnikova, H. N. Ananthaswamy, *Mutat. Res.* **571**, 91 (2005).
5. M. M. Becker, J. C. Wang, *Nature* **309**, 682 (1984).
6. J. M. Gale, K. A. Nissen, M. J. Smerdon, *Proc. Natl. Acad. Sci. U.S.A.* **84**, 6644 (1987).
7. J. R. Pehrson, *Proc. Natl. Acad. Sci. U.S.A.* **86**, 9149 (1989).
8. F. Bernardi, S. De, M. Olivucci, M. A. Robb, *J. Am. Chem. Soc.* **112**, 1737 (1990).
9. P. J. Wagner, *Acc. Chem. Res.* **16**, 461 (1983).
10. C. E. Crespo-Hernández, B. Cohen, P. M. Hare, B. Kohler, *Chem. Rev.* **104**, 1977 (2004).
11. C. E. Crespo-Hernández, B. Cohen, B. Kohler, *Nature* **436**, 1141 (2005).
12. P. M. Hare, C. E. Crespo-Hernández, B. Kohler, *Proc. Natl. Acad. Sci. U.S.A.* **104**, 435 (2007).
13. S. Marguet, D. Markovitsi, *J. Am. Chem. Soc.* **127**, 5780 (2005).
14. M. K. Kuimova *et al.*, *Proc. Natl. Acad. Sci. U.S.A.* **103**, 2150 (2006).
15. Materials and methods are available as supporting material on *Science* Online.
16. Z. Tramer, K. L. Wierzchowski, D. Shugar, *Acta Biochim. Pol.* **16**, 83 (1969).
17. T. Douki, *J. Photochem. Photobiol. B Biol.* **82**, 45 (2006).
18. S. I. Zhang, K. H. Michaelian, G. R. Loppnow, *J. Phys. Chem. A* **102**, 461 (1998).
19. I. H. M. van Stokkum, D. S. Larsen, R. van Grondelle, *Biochim. Biophys. Acta Bioenerg.* **1657**, 82 (2004).
20. D. L. Mitchell, J. M. Clarkson, *Photochem. Photobiol.* **40**, 735 (1984).
21. J. Butenandt, A. P. M. Eker, T. Carell, *Chem. Eur. J.* **4**, 642 (1998).
22. T. Schrader *et al.*, *Chem. Phys. Lett.* **392**, 358 (2004).
23. T. Q. Lian, B. Locke, Y. Kholodenko, R. M. Hochstrasser, *J. Phys. Chem.* **98**, 11648 (1994).
24. R. A. Deering, R. B. Setlow, *Biochim. Biophys. Acta* **68**, 526 (1963).
25. N. F. Scherer, C. Sipes, R. B. Bernstein, A. H. Zewail, *J. Chem. Phys.* **92**, 5239 (1990).
26. W. Fuß, K. K. Pushpa, W. E. Schmid, S. A. Trushin, *Photochem. Photobiol. Sci.* **1**, 60 (2002).
27. J. M. Martinez, S. K. C. Elmroth, L. Kloo, *J. Am. Chem. Soc.* **123**, 12279 (2001).
28. R. O. Rahn, *Science* **154**, 503 (1966).
29. M. M. Becker, Z. Wang, *J. Mol. Biol.* **210**, 429 (1989).
30. R. O. Rahn, J. L. Hosszu, *Photochem. Photobiol.* **7**, 637 (1968).
31. R. Lisewski, K. L. Wierzchowski, *Photochem. Photobiol.* **11**, 327 (1970).
32. A. A. Lamola, J. Eisinger, *Proc. Natl. Acad. Sci. U.S.A.* **59**, 46 (1968).
33. J. B. Mills, E. Vacano, P. J. Hagerman, *J. Mol. Biol.* **285**, 245 (1999).
34. H. Park *et al.*, *Proc. Natl. Acad. Sci. U.S.A.* **99**, 15965 (2002).
35. J. L. Hosszu, R. O. Rahn, *Biochem. Biophys. Res. Commun.* **29**, 327 (1967).
36. W. Saenger, *Principles of Nucleic Acid Structure* (Springer-Verlag, Berlin, 1984).
37. M. M. Becker, W. Zhou, *J. Biol. Chem.* **264**, 4163 (1989).
38. L. M. Kundu, U. Linne, M. Marahiel, T. Carell, *Chem. Eur. J.* **10**, 5697 (2004).
39. V. Lyamichev, *Nucleic Acids Res.* **19**, 4491 (1991).

40. B.K. thanks NIH (grant GM064563) and the Alexander von Humboldt Foundation for support.

Supporting Online Material

www.sciencemag.org/cgi/content/full/315/5812/625/DC1
Materials and Methods
Figs. S1 and S2
References

21 September 2006; accepted 5 December 2006
10.1126/science.1135428

Single Photon–Induced Symmetry Breaking of H_2 Dissociation

F. Martín,[1] J. Fernández,[1] T. Havermeier,[2] L. Foucar,[2] Th. Weber,[2] K. Kreidi,[2] M. Schöffler,[2] L. Schmidt,[2] T. Jahnke,[2] O. Jagutzki,[2] A. Czasch,[2] E. P. Benis,[3] T. Osipov,[4] A. L. Landers,[5] A. Belkacem,[4] M. H. Prior,[4] H. Schmidt-Böcking,[2] C. L. Cocke,[3] R. Dörner[2]*

H_2, the smallest and most abundant molecule in the universe, has a perfectly symmetric ground state. What does it take to break this symmetry? We found that the inversion symmetry can be broken by absorption of a linearly polarized photon, which itself has inversion symmetry. In particular, the emission of a photoelectron with subsequent dissociation of the remaining H_2^+ fragment shows no symmetry with respect to the ionic H^+ and neutral H atomic fragments. This lack of symmetry results from the entanglement between symmetric and antisymmetric H_2^+ states that is caused by autoionization. The mechanisms behind this symmetry breaking are general for all molecules.

Symmetries are essential building blocks of our physical, chemical, and biological models. For macroscopic objects, symmetries are always only approximate. By reducing the complexity in the microcosm, these symmetries often become strict. Thus, in any symmetric molecule, the ground state has a well-defined parity. This property has far-reaching consequences, such as truncation of rotational spectra or the existence of ortho- and para-molecular isomers (*1*). One way to break the symmetry is isotopic substitution of one of the nuclei (*2*). In larger systems, symmetry breaking can also be achieved through selected vibrational modes, such as asymmetric stretch, which lies at the origin of the Jahn-Teller and Rener-Teller effects (*3*). Alternatively, external fields can be used to favor a particular molecular direction, a method that has recently been used by Kling *et al*. (*4*) to induce asymmetric dissociation of the H_2^+ molecular ion into a proton and a hydrogen atom. Here, we show that, in dissociative ionization by absorption of a single photon

$$h\nu + H_2 \rightarrow p + H + e^- \qquad (1)$$

symmetry breaking is possible even in the absence of an external field. This is the smallest and most fundamental molecular system for which such symmetry breaking is possible.

Symmetry operations in a molecule that has a well-defined parity can change the sign of the ground state wave function (odd parity, or ungerade, states). However, all observables must be symmetric, because they are squares of wave functions or transition matrix elements. To achieve left-right asymmetry in an observable, the system must be put into a coherent superposition of gerade (g) (even) and ungerade (u) (odd) molecular states. The relative phase between the two states can then lead to a left or right localization of an electron. Direct photoionization usually cannot induce this outcome, because the g and u states of the remaining molecular ion have different energies. Therefore, two ionization pathways are distinguishable by the electron energy and hence the coherence is lost.

Figure 1A shows the energy diagram for the H_2 and H_2^+ molecules. The energy difference between the lowest g and u states in H_2^+, $^2\Sigma_g^+(1s\sigma_g)$ and $^2\Sigma_u^+(2p\sigma_u)$, respectively, is about 17 eV in the Franck-Condon region of H_2. Thus, if H_2 is directly ionized in a vertical transition by a photon of energy $h\nu$, the photoelectron will have an energy of about $E_e = h\nu - 16$ eV when the remaining H_2^+ is in the g state, whereas it will have $E_e = h\nu - 33$ eV when the remaining H_2^+ is in the repulsive u state. Both ionization paths are distinguishable by the energy (Fig. 1, B and C). Because in either path H_2^+ is in a state of well-defined parity, it manifests no memory of the direction toward

[1]Departamento de Química, C-9, Universidad Autónoma de Madrid, 28049 Madrid, Spain. [2]Institut für Kernphysik, University Frankfurt, Max von Laue Strasse 1, D-60438 Frankfurt, Germany. [3]Department of Physics, Kansas State University, Cardwell Hall, Manhattan, KS 66506, USA. [4]Lawrence Berkeley National Laboratory, Berkeley, CA 94720, USA. [5]Department of Physics, Auburn University, Auburn, AL 36849, USA.

*To whom correspondence should be addressed. E-mail: doerner@atom.uni-frankfurt.de

which the photoelectron is emitted. We show that such a memory becomes possible if indirect pathways of ionization through doubly excited states are taken into account (Fig. 1, D and E).

The quantum dynamics of the population and decay of doubly excited states presents an important and fundamental challenge to theory. The full four-body problem must be treated entirely with quantum mechanics, without semiclassical approximations for the nuclear motion. Our ab initio calculation meets this challenge. In the accompanying kinematically complete experiment, we used cold target recoil ion momentum spectroscopy (COLTRIMS) (*5*, *6*) to provide the most detailed possible check of this theory. We calculated and measured the vector momenta of the proton and the ejected electron in coincidence. Because the dissociation is rapid compared with molecular rotation, the direction of fragmentation coincides with the molecular orientation at the instant of electron emission. Thus, measurements of the electron angular distribution afford data in the body-fixed frame of the molecule, and asymmetry in the molecular dissociation can be observed with respect to the electron direction.

Doubly excited states and their decay give rise to a multitude of narrow structures, called Fano resonances (*7*), in atomic photoionization spectra. These oscillations in the cross-section are the result of interference between two indistinguishable pathways through which the electron can be ejected. The photon can expel an electron directly, or it can promote the atom to a doubly excited state, which then decays after a delay caused by emission of one electron through autoionization. Because the final state in both of these pathways is the same, the amplitudes for each pathway must be added coherently, leading to either constructive or destructive interference, depending on the phase shift induced by the time delay. Doubly excited states have also been seen (*8*–*11*) and predicted (*12*, *13*) for molecules. However, because in molecules the excess photon energy can be distributed among internal nuclear and electron degrees of freedom, the situation is much more complex than in atoms, and a clear-cut proof of the interference effects is missing.

We clearly demonstrate such interference effects and show that they cause symmetry breaking in dissociative photoionization. A first observation of asymmetric photoelectron emission from H_2 has been reported in pioneering experiments by Lafosse *et al*. (*14*). In a different context, asymmetric electron emission has been observed in O_2 (*15*) as the result of the decay of atomic oxygen after photodissociation of the O_2 molecule. In this case, the observed asymmetry thus does not strictly arise from a molecular decay process.

We used the framework of the dipole approximation given in Dill's formula (*16*) to evaluate photoionization cross-sections that correspond to leaving the residual molecular ion in a specific electronic state α, which is differential in (i) the photoelectron energy ε, (ii) the photoelectron emission direction in the molecular frame, and (iii) the polarization direction with respect to the molecular axis. The transition matrix element involves the ground molecular state of energy W_{gv} and the final molecular state of energy $W_{\upsilon_\alpha} + \varepsilon$ representing a molecular ion in the υ_α vibronic state (either dissociative or nondissociative) and an emitted electron of energy ε. Energy conservation dictates that $W_{gv} + h\nu = W_{\upsilon_\alpha} + \varepsilon$. The two wave functions were connected by the dipole operator and were evaluated, neglecting rotational effects, in the adiabatic approximation using the theory of Sánchez and Martín (*17*). [See also equations 42 and 60 of Martín (*18*).]

Briefly, the final state comes from a close-coupling calculation incorporating contributions from the two lowest ionization thresholds of H_2 [$^2\Sigma_g^+(1s\sigma_g)$ and $^2\Sigma_u^+(2p\sigma_u)$], the six lowest

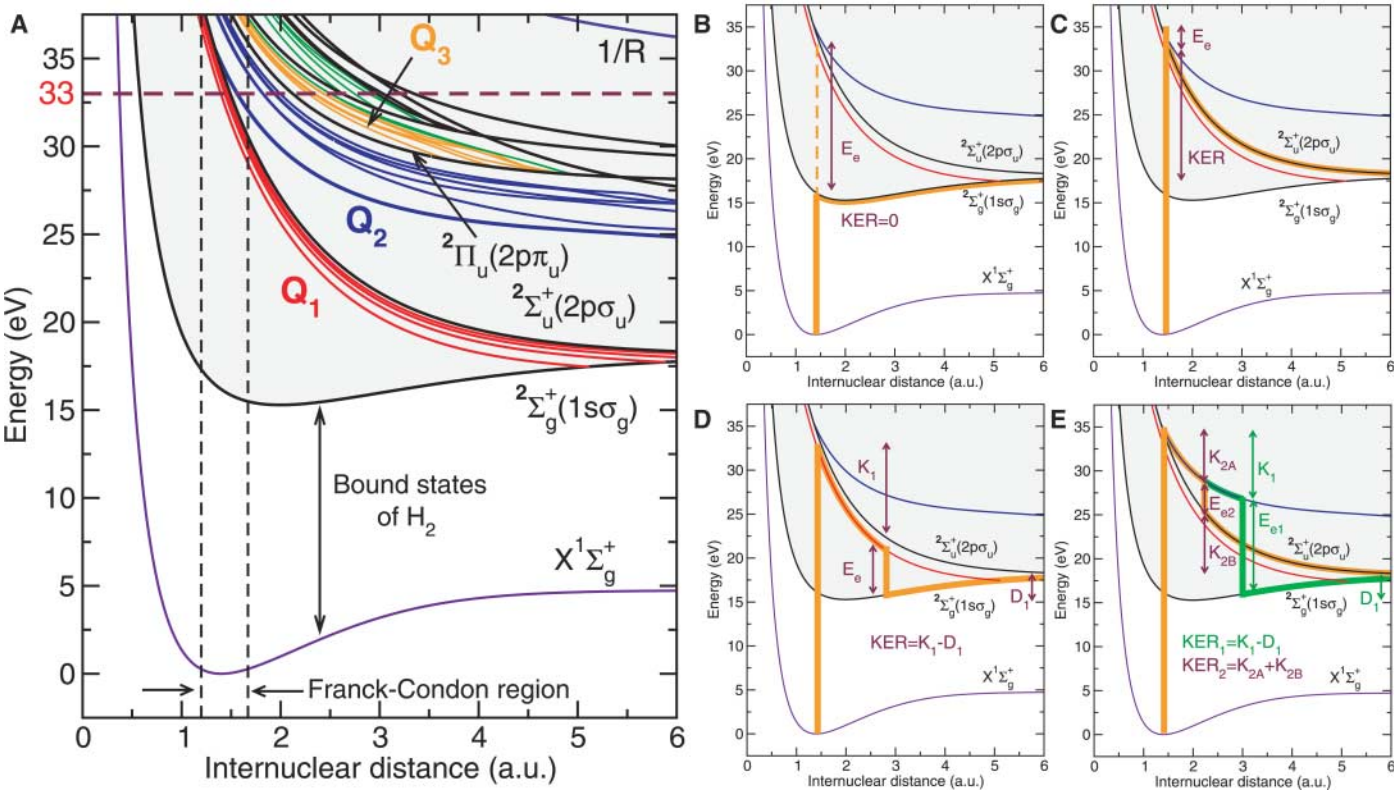

Fig. 1. Energy-level diagram and pathways to dissociative ionization. (**A**) Total energy of the H_2 and H_2^+ systems as a function of internuclear distance (a.u., atomic units). Red and blue are the lowest two series of doubly excited states of H_2 with $^1\Pi_u$ symmetry. At large internuclear distances, the Q_1 states dissociate into H(n = 1) + H(n = 2,...,∞) and the Q_2 states into H(n = 2, l = 1) + H(n = 2,...,∞), where n and l are, respectively, the principal and angular momentum quantum numbers of the state. (**B** to **E**) Semiclassical pathways for dissociative ionization by absorption of one 33-eV photon. (B) Direct ionization leading to $H_2^+(1s\sigma_g)$ (Eq. 2). (C) Direct ionization leading to $H_2^+(2p\sigma_u)$ (Eq. 3). (D) Resonant ionization through the lowest Q_1 doubly excited states leading to $H_2^+(1s\sigma_g)$ (Eq. 4). (E) Resonant ionization through the lowest Q_2 doubly excited states leading to $H_2^+(1s\sigma_g)$ (Eq. 5) or to $H_2^+(2p\sigma_u)$ (Eq. 6).

doubly excited states of the Q_1 and Q_2 series for both Σ_u^+ and Π_u symmetries, and the corresponding vibrational and dissociative states. At variance with dissociative states associated with bound electronic states, those associated with doubly excited states are the solutions of a complex nonlocal differential equation that includes the possibility of autoionization decay as the molecule dissociates. Therefore, the final state wave function is not given simply by the product of an electronic and a nuclear wave function but by a more complex form that accounts for interferences among the various electronic and nuclear channels. The theory is formally exact within the adiabatic and nonrotation approximations provided that all electronic and nuclear differential equations are solved exactly (*18*).

Our computational methods used B-spline functions to obtain the electronic and vibrational wave functions and are similar to methods successfully applied to a variety of other dissociation-ionization problems in H_2 (*13*, *19*, *20*). B-spline functions have also, within the fixed-nuclear approximation, led to the first numerical solution of the double photoionization of H_2 (*21*).

The experiments were performed at beamline 9.3.2 of the Advanced Light Source at Lawrence Berkeley National Laboratory. The monochromatized linearly polarized light from the synchrotron was crossed with an internally cold and localized supersonic H_2 and D_2 gas jet. The ions and electrons were directed by a combination of weak electric (20 V/cm) and parallel magnetic (10 G) fields onto two position-sensitive microchannel plate detectors with delay-line position encoding (*22*). Vector momenta were calculated from the position of impact and the times of flight of each particle. The energies of both ions and electrons were measured. Electron, ion, and neutral fragment momenta k_e, k_p^+, and k_H, respectively, are related by momentum conservation: $k_e = -(k_p^+ + k_H)$. Because of the light electron mass, the electron momentum is about 2.5% of the heavy particle momentum, leading to a nearly back-to-back fragmentation of the proton and hydrogen atom. The energy deposited by the photon ($h\nu$) in excess of the threshold for dissociative ionization (18.1 eV, Eq. 1) is partitioned among the kinetic energy release (KER) of the heavy fragments, the electron energy (E_e), and internal excitation energy (E_{exc}) of the neutral ($h\nu = KER + E_e - 18.1\ \text{eV} - E_{exc}$). As expected, the hydrogen atom is found only in the ground state ($E_{exc} = 0$) in the photon energy range that we examined. The asymptote of the $1s\sigma_g$ and $2p\sigma_u$ curve in Fig. 1 corresponds to a proton and a hydrogen atom in its ground state. Because both KER and E_e were measured for each event, energy conservation could be used to very efficiently suppress random background or proton and electron pairs from residual water molecules in the chamber. The overall energy resolution was between 100 meV and 0.5 eV, depending on the energy, and the angular resolution was about 5°. More detail on the COLTRIMS system can be found in Jahnke *et al.* (*23*).

For simplicity, we restrict our discussion to an orientation of the molecule perpendicular to the polarization axis. This orientation selects transitions from the ground state of Σ_g^+ symmetry to excited states of Π_u symmetry. Figure 2 shows the KER distribution for the reaction in Eq. 1 as a function of the photon energy. Three areas with islands can be distinguished (I, II, and III in Fig. 2B): Regions I and III can be populated by direct ionization, leaving H_2^+ in the $2p\sigma_u$ or $1s\sigma_g$ state, respectively. However, only the latter state contributes substantially, because a direct dipole transition from the H_2 ground state to the $2p\sigma_u k\pi_g$ continuum is very unlikely (*13*). [Indeed, it would be strictly forbidden in an independent electron picture, $(1s\sigma_g)^2 \rightarrow 2p\sigma_u k\pi_g$.] Thus, regions I and II cannot be reached in a single-step direct photoionization. They are the fingerprint of a delayed emission of an Auger electron from H_2 doubly excited states (either Q_1 or Q_2). These states can either dissociate as a result of the repulsive character of the corresponding potential energy curve or decay by autoionization into the $2p\sigma_u$ or $1s\sigma_g$ states when such a decay is faster than the time required for an effective dissociation.

We distinguished five different pathways, all contributing to ionization in the photon energy range of Fig. 2 and schematically shown in Fig. 1, B to E:

$$h\nu + H_2 \rightarrow H_2^+(1s\sigma_g) + e^-, \text{ direct} \quad (2)$$

$$h\nu + H_2 \rightarrow H_2^+(2p\sigma_u) + e^-, \text{ direct} \quad (3)$$

$$h\nu + H_2 \rightarrow H_2(Q_1) \rightarrow H_2^+(1s\sigma_g) + e^-, \text{ resonant} \quad (4)$$

$$h\nu + H_2 \rightarrow H_2(Q_2) \rightarrow H_2^+(1s\sigma_g) + e^-, \text{ resonant} \quad (5)$$

$$h\nu + H_2 \rightarrow H_2(Q_2) \rightarrow H_2^+(2p\sigma_u) + e^-, \text{ resonant} \quad (6)$$

Asymptotically, $H_2^+(2p\sigma_u)$ always leads to a dissociation, whereas $H_2^+(1s\sigma_g)$ can lead either to H_2^+ in a bound vibrational state or to a dissociative state. All of these pathways must be added coherently when they yield the same electron energy and hence the same KER. Their interference leads to the distinct finger-like structures in the low KER region (Fig. 2, C to F). The calculated structures (Fig. 2, C and E) are in excellent agreement with the experimental observations (Fig. 2, D and F). Our calculations show that the structure is the result of an interference between the processes in Eqs. 2 and 4, the direct and resonant pathways leading to $1s\sigma_g$

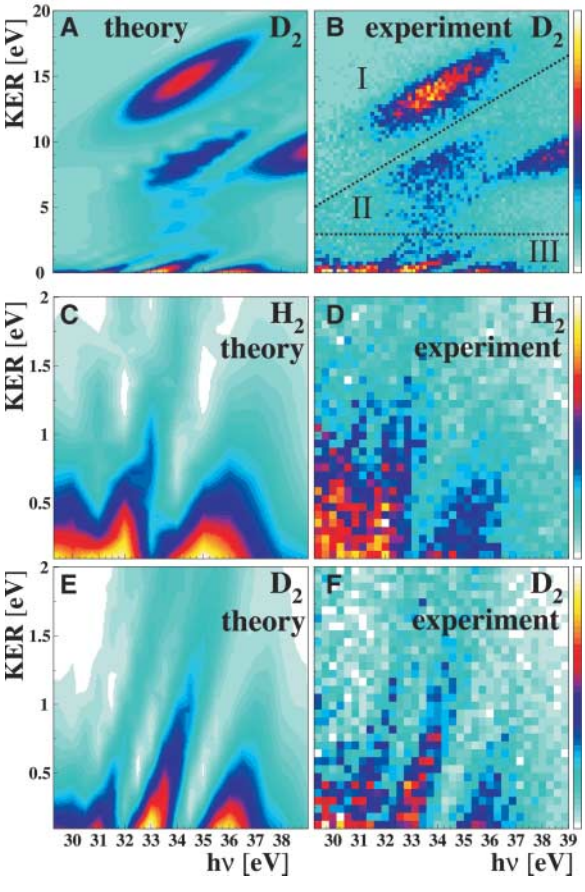

Fig. 2. Kinetic energy release as a function of photon energy for dissociative ionization of H_2 and D_2 (Eq. 1). (**A**) Theory and (**B**) experiment for D_2. Regions I, II, and III show three distinct clusters of data formed by photoionization. (**C** to **F**) Magnification of the low-KER region of panels (A) and (B) for H_2 [(C) and (D)] and D_2 [(E) and (F)]. Left, theory; right, experiment.

in the same KER region. The finger-like structures are the molecular analog of the well-known Fano interferences in the atomic case, but there are important differences entirely due to the molecular character of H_2. As the photon energy increases, the position of a particular peak shifts to higher KER, which leads to fingers with a slope approximately equal to one. The number and position of the fingers is controlled by the overlap between the dissociative states that are associated, respectively, with processes in Eqs. 2 and 4, so it is not surprising that our experimental data and calculations for H_2 and D_2 show a large isotope effect on these structures (the different masses cause distinct oscillations in the dissociative states).

We then turned to the angular distribution of the electron. We considered a photon energy of 33.25 eV and, as above, an orientation of the molecule perpendicular to the polarization axis. Figure 3 shows the key results of this work. Plotted is the angular distribution of the electron with respect to the polarization axis (horizontal). The plane of the figure is defined by the molecular axis and the polarization vector; only electrons in this plane are selected. The molecule is perpendicular to the polarization axis with the proton pointing upward. The angular distributions are found to vary strongly with the kinetic energy release. In addition to the change from a dumbbell to a butterfly shape, we found a strong asymmetry, in particular in a narrow range of $KER \cong 8$ to 10 eV, corresponding to an electron energy of $E_e \cong 5$ to 7eV. All major features predicted by our theory are confirmed by the experimental data. They are also consistent with those reported in a previous experiment (*14*) by averaging over KER intervals of 2.5 to 3 eV.

Our theoretical analysis allows us to distinguish the contributions leading to $1s\sigma_g$ (the sum of processes in Eqs. 2, 4, and 5) from those leading to $2p\sigma_u$ (the sum of processes in Eqs. 3 and 6). For a fixed photon energy of 33.25 eV, the contributions of the $1s\sigma_g$ and $2p\sigma_u$ channels overlap in the 8- to 10-eV region (Fig. 4), where the largest asymmetry is observed (Fig. 3).

How can the $1s\sigma_g$ and $2p\sigma_u$ channels interfere to produce an asymmetric angular distribution? To answer this question, we performed a model calculation in which we only included the direct ionization channels—$1s\sigma_g k\pi_u$ and $2p\sigma_u k\pi_g$—and the lowest Q_2 state of Π_u symmetry. The angular distributions found in this model calculation were very similar to those obtained from the full calculation (Fig. 3). In particular, the asymmetry was very well reproduced, showing that the Q_1 states are not responsible for its occurrence. We then excluded the two direct channels (Eqs. 2 and 3) and only considered the decay of the Q_2 state through the channels in Eqs. 5 and 6. The asymmetry remained, thus showing that the origin of the asymmetry is the interference between these two channels, i.e., between the resonant population of an ungerade and a gerade state. It is only the coherent superposition of these pathways that allows for a localization of the bound electron in the dissociating H_2^+. The transient molecule has broken symmetry and can keep a memory of the direction in which the electron departed. We also found that the fingers in Fig. 2 did not appear when the direct channel (Eq. 2) was not included in the calculation, thus confirming that their origin is the interference between resonant and nonresonant population of the $1s\sigma_g$ state. In any case, the latter interference did not lead to a noticeable asymmetry.

The results of the full quantum calculation completely differed from those of the widely used simple semiclassical model (also used in Fig. 1, B to E, for pedagogical purposes). In this simple model, the system always strictly followed the potential energy curves and only vertical transitions between them were allowed. These vertical transitions may occur as a result of photon absorption (vertical lines on the left) or autoionization decay (vertical lines on the right). In this framework, all molecules had an

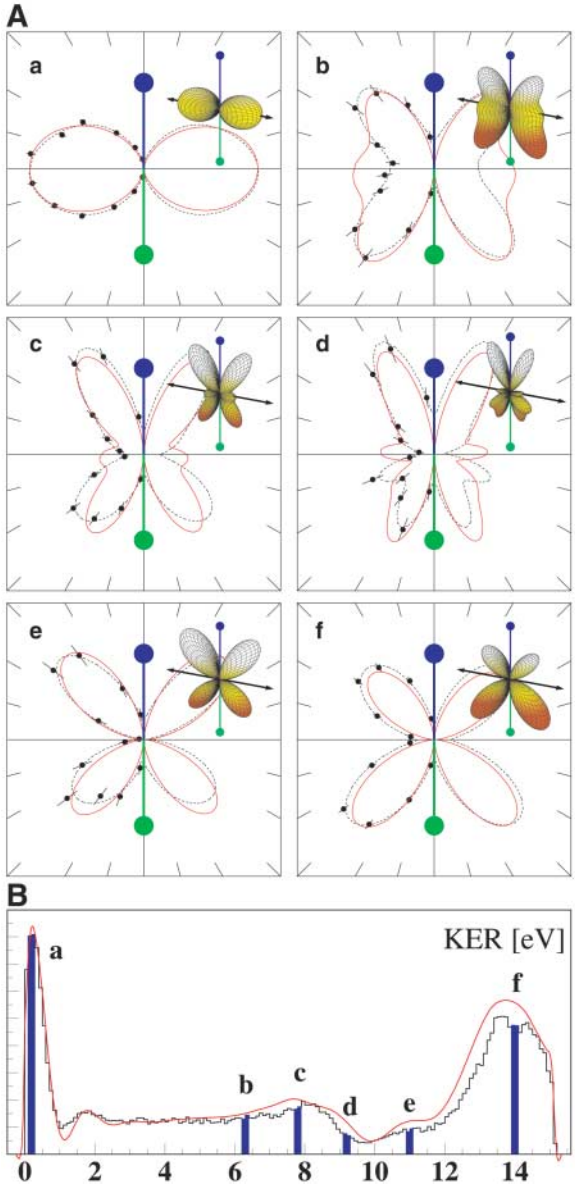

Fig. 3. (**A**) Angular distribution of the electrons as a function of KER for dissociative ionization of D_2 (Eq. 1) at a photon energy of 33.25 eV, linearly polarized light. The orientation of the molecule at 90° to the polarization (theory) and 90° ± 10° (experiment) is indicated by colored circles (blue, deuteron; green, deuterium). The (horizontal) polarization vector and the molecular axis define a common plane. The electron is restricted to this plane by ±45°. Solid red line, theory; circles with error bars (where error is SD), experiment; dotted line, fit of the experimental data with spherical harmonics. The theoretical results have been integrated over the experimental acceptance angles and KER resolution as well as electron resolution. Infinite resolution theoretical results are shown by the small three-dimensional plots in the upper right: KER = 0.2 (a), 6.3 (b), 7.8 (c), 9.2 (d), 11 (e), and 14 eV (f). Units are arbitrary units. (**B**) The angle-integrated KER spectrum. Red line, theory; black line, experiment; letters a to f correspond to a to f in (A); KER intervals are ±0.1 eV. The *x*-axis shows KER in eV. The *y*-axis shows a cross-section in arbitrary units.

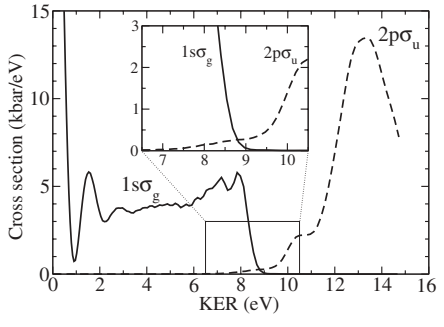

Fig. 4. Calculated D^+ kinetic energy distribution in dissociative ionization of D_2 by absorption of a 33.25-eV photon. Solid line, $1s\sigma_g$ channel; dashed line, $2p\sigma_u$ channel. The inset is a magnification of the squared region.

identically well-defined value of the internuclear distance during the transition and, consequently, any possible direct energy exchange between electronic and nuclear motions was neglected. For example, in such a model, the electron energy from the path shown by an orange line in Fig. 1E (resonant photoionization through the $2p\sigma_u$ channel) would be equal to the energy difference between the Q_2 and the $2p\sigma_u$ curve at the marked internuclear distance. Similar reasoning predicts the electron energy along the path shown by the green line (resonant photoionization through the $1s\sigma_g$ channel). Our calculations show that, in this case, although such simplified models have heuristic and pedagogical value, they lead to false conclusions. The model predicts that the maximum possible value of the KER in the $1s\sigma_g$ channel is 8.1 eV (corresponding to an autoionization decay at infinite internuclear distance), which is the minimum possible value of the KER in the $2p\sigma_u$ channel (corresponding to autoionization decay at the equilibrium internuclear distance). Therefore, no interference between g and u states can occur within this model because the electron energies and the KER regions for transitions to $1s\sigma_g$ and $2p\sigma_u$ would have no overlap, and hence the electron ejection would always be symmetric. Our fully quantum mechanical treatment showed that transitions to the $1s\sigma_g$ state can occur beyond 8.1 eV and that transitions to the $2p\sigma_u$ state are possible even at zero KER. Thus, the angular distribution can exhibit an asymmetry over the whole region of KER. Strictly speaking, a symmetric dissociation in the presence of resonances is the exception rather than the rule. It becomes quantitatively substantial in the region where both channels are comparably active, between 8 and 10 eV; however, it is also visible in regions where one of the channels dominates (Fig. 3A, b to f).

Notably, the observed asymmetry has no relation to the direction in which the charged fragment is emitted: The larger lobes are sometimes found on the ion side (Fig. 3A, c, d, and e) and sometimes on the neutral side (Fig. 3A, b and f). Both theory and experiment show that the asymmetry oscillates with the KER and that the amplitude of these oscillations is more important in the region where the $1s\sigma_g$ and $2p\sigma_u$ channels overlap. Between consecutive oscillations, there are KER values for which the distribution is practically symmetric. Thus, the asymmetry cannot be explained by a preferred attractive interaction between the proton and the escaping electron (the latter is too fast to be efficiently perturbed by the slow proton, except possibly in the region of the maximum allowed KER).

Asymmetric photoelectron angular distributions should arise in any symmetric molecule that decays through two (or more) dissociative ionization channels associated with different symmetries of the residual molecular ion. When the final electron energy is the same in both channels, the corresponding ionization pathways are indistinguishable. This equivalence leads to interferences that depend on the time delay between the two ionization processes. The time delay implies that the decay in either pathway occurs at different positions of the nuclei. This unique relationship between time delay and nuclear positions makes the problem of molecular autoionization much richer than the atomic case, and the asymmetry of the photoelectron angular distribution its most noteworthy (and so far unexpected) effect. Symmetry breaking should be considered a general molecular manifestation of autoionization when several decay channels are effectively accessible.

References and Notes

1. I. N. Levine, *Molecular Spectroscopy* (Wiley, New York, 1975).
2. D. Rolles *et al.*, *Nature* **437**, 711 (2005).
3. G. Herzberg, *Molecular Spectra and Molecular Structure*, vol. III of *Electronic Spectra and Electronic Structure of Polyatomic Molecules* (Prentice-Hall, New York, 1979).
4. M. F. Kling *et al.*, *Science* **312**, 246 (2006).
5. R. Dörner *et al.*, *Phys. Rep.* **330**, 95 (2000).
6. J. Ullrich *et al.*, *Rep. Prog. Phys.* **66**, 1463 (2003).
7. U. Fano, *Phys. Rev.* **124**, 1866 (1961).
8. S. Strathdee, R. Browning, *J. Phys. B* **12**, 1789 (1979).
9. C. J. Latimer, J. Geddes, M. A. McDonald, N. Kouchi, K. F. Dunn, *J. Phys. B* **29**, 6113 (1996).
10. K. Ito, R. I. Hall, M. Ukai, *J. Chem. Phys.* **104**, 8449 (1996).
11. M. Lebech *et al.*, *Phys. Rev. Lett.* **96**, 073001 (2006).
12. C. Bottcher, K. Docken, *J. Phys. B* **7**, L5 (1974).
13. I. Sánchez, F. Martín, *Phys. Rev. A.* **60**, 2200 (1999).
14. A. Lafosse *et al.*, *J. Phys. B* **36**, 4683 (2003).
15. A. V. Golovin *et al.*, *Phys. Rev. Lett.* **79**, 4554 (1997).
16. D. Dill, *J. Chem. Phys.* **65**, 1130 (1976).
17. I. Sánchez, F. Martín, *Phys. Rev. Lett.* **82**, 3775 (1999).
18. F. Martín, *J. Phys. B* **32**, R197 (1999).
19. H. Bachau, E. Cormier, P. Decleva, J. E. Hansen, F. Martín, *Rep. Prog. Phys.* **64**, 1815 (2001).
20. G. Laurent *et al.*, *Phys. Rev. Lett.* **96**, 173201 (2006).
21. W. Vanroose, F. Martín, T. N. Rescigno, C. W. McCurdy, *Science* **310**, 1787 (2005).
22. O. Jagutzki *et al.*, *Nucl. Instrum. Methods* **A477**, 244 (2002).
23. T. Jahnke *et al.*, *J. Electron Spectrosc. Relat. Phenom.* **141**, 229 (2004).

24. This work was supported in part by Dirección General de Investigación project no. BFM2003-00194; the European Cooperation in the field of Scientific and Technical Research (COST) action D26/0002/02; Bundesministerium für Bildung und Forschung; Deutsche Forschungsgemeinschaft; Deutscher Akademischer Austauschdienst; the Division of Chemical Sciences, Geosciences and Biosciences Division, Office of Basic Energy Sciences, Office of Science, U.S. Department of Energy; and the Director, Office of Science, Office of Basic Energy Sciences and Division of Materials Sciences under U.S. Department of Energy contract no. DE-AC03-76SF00098. We thank Roentdek GmbH (www.roentdek.com) for support with the delay-line detectors; the Centro de Computación Científica of the Universidad Autónoma de Madrid for its generous allocation of computer time; D. Dowek for discussions related to the effects observed in her group; H. J. Lüdde for discussions; and the staff at Advanced Light Source, in particular B. S. Mun, for support.

23 October 2006; accepted 8 December 2006
10.1126/science.1136598

Ultrafast Bond Softening in Bismuth: Mapping a Solid's Interatomic Potential with X-rays

D. M. Fritz,[1,2*] D. A. Reis,[1,2] B. Adams,[3] R. A. Akre,[4] J. Arthur,[5] C. Blome,[6] P. H. Bucksbaum,[2,4,7] A. L. Cavalieri,[8] S. Engemann,[5] S. Fahy,[9] R. W. Falcone,[10] P. H. Fuoss,[11] K. J. Gaffney,[5] M. J. George,[5] J. Hajdu,[12] M. P. Hertlein,[13] P. B. Hillyard,[14] M. Horn-von Hoegen,[15] M. Kammler,[16] J. Kaspar,[14] R. Kienberger,[8] P. Krejcik,[4] S. H. Lee,[17] A. M. Lindenberg,[5] B. McFarland,[7] D. Meyer,[15] T. Montagne,[4] É. D. Murray,[9] A. J. Nelson,[18] M. Nicoul,[15] R. Pahl,[19] J. Rudati,[3] H. Schlarb,[6] D. P. Siddons,[20] K. Sokolowski-Tinten,[15] Th. Tschentscher,[6] D. von der Linde,[15] J. B. Hastings[5]

Intense femtosecond laser excitation can produce transient states of matter that would otherwise be inaccessible to laboratory investigation. At high excitation densities, the interatomic forces that bind solids and determine many of their properties can be substantially altered. Here, we present the detailed mapping of the carrier density–dependent interatomic potential of bismuth approaching a solid-solid phase transition. Our experiments combine stroboscopic techniques that use a high-brightness linear electron accelerator–based x-ray source with pulse-by-pulse timing reconstruction for femtosecond resolution, allowing quantitative characterization of the interatomic potential energy surface of the highly excited solid.

The availability of bright sources of ultrafast hard x-rays, such as future free-electron lasers, opens up the possibility to follow atomic motion stroboscopically with the picometer spatial and femtosecond temporal resolution required to capture the fastest atomic vibrations and the making and breaking of chemical bonds (*1*). However, the inability to precisely time the x-ray probe can lead to significant reduction in temporal resolution. Recently, the use of single-shot determination of the x-ray arrival time as a means of random sampling has been demonstrated to circumvent this problem (*2*). Using this technique, we con-